

Impacts of viscous dissipation on collisional growth and fragmentation of dust aggregates

SOTA ARAKAWA ^{1,2}, HIDEKAZU TANAKA ³, AND EIICHIRO KOKUBO ¹

¹National Astronomical Observatory of Japan, 2-21-1, Osawa, Mitaka, Tokyo, 181-8588, Japan

²Japan Agency for Marine-Earth Science and Technology, 3173-25, Showa-machi, Kanazawa-ku, Yokohama, 236-0001, Japan

³Astronomical Institute, Graduate School of Science Tohoku University, 6-3 Aramaki, Aoba-ku, Sendai 980-8578, Japan

Submitted to ApJ

ABSTRACT

Understanding the collisional behavior of dust aggregates consisting of submicron-sized grains is essential to unveiling how planetesimals formed in protoplanetary disks. It is known that the collisional behavior of individual dust particles strongly depends on the strength of viscous dissipation force; however, impacts of viscous dissipation on the collisional behavior of dust aggregates have not been studied in detail, especially for the cases of oblique collisions. Here we investigated the impacts of viscous dissipation on the collisional behavior of dust aggregates. We performed numerical simulations of collisions between two equal-mass dust aggregates with various collision velocities and impact parameters. We also changed the strength of viscous dissipation force systematically. We found that the threshold collision velocity for the fragmentation of dust aggregates barely depends on the strength of viscous dissipation force when we consider oblique collisions. In contrast, the size distribution of fragments changes significantly when the viscous dissipation force is considered. We obtained the empirical fitting formulae for the size distribution of fragments for the case of strong dissipation, which would be useful to study the evolution of size and spatial distributions of dust aggregates in protoplanetary disks.

1. INTRODUCTION

Collisional evolution of dust aggregates consisting of submicron-sized grains in protoplanetary disks is the first step of the planet formation (e.g., Johansen et al. 2014). To make planetesimals, dust aggregates should grow through collisions; however, the condition for collisional growth of dust aggregates is still under debate.

In protoplanetary disks, the gas drag transfers the angular momentum and causes the radial drift of dust aggregates. In the minimum mass solar nebula model (Hayashi 1981), the dust aggregates drift inwardly with the radial drift velocity of approximately 50 m s^{-1} at the maximum (Adachi et al. 1976; Weidenschilling 1977). Since the radial drift velocity depends on the size of dust aggregates, two dust aggregates with different size have a relative velocity due to radial drift motion. The collision velocity of dust aggregates is also provided by the influence of gas turbulence (e.g., Ormel & Cuzzi 2007; Sakurai et al. 2021). The maximum velocity caused by radial drift and turbulence is typically $10\text{--}100 \text{ m s}^{-1}$ at $3\text{--}5 \text{ au}$ from the central star (e.g., Hasegawa et al. 2021). Therefore, understanding the collisional behavior of dust aggregates for the collision velocity lower than 100 m s^{-1} is essential to investigate how dust aggregates evolve into planetesimal in protoplanetary disks. We note that the strength

of gas turbulence would be related to the size and spatial distributions of dust aggregates in protoplanetary disks (e.g., Okuzumi & Hirose 2012), and the size distribution of fragments produced via collisions is important to constrain the collisional growth paths of dust aggregates.

The collisional behavior of dust aggregates has been reported in a large number of studies based on both laboratory experiments (e.g., Blum & Wurm 2008; Güttler et al. 2010; Shimaki & Arakawa 2012; Brisset et al. 2016, 2017; Schräpler et al. 2018, 2022; Fritscher & Teiser 2021) and numerical simulations (e.g., Wada et al. 2007, 2008, 2009, 2013; Paszun & Dominik 2009; Seizinger et al. 2013; Sirono & Ueno 2017; Umstätter & Urbassek 2020, 2021a; Hasegawa et al. 2021; Sirono & Kudo 2021). It is known that the threshold collision velocity for the fragmentation of dust aggregates, v_{fra} , depends on material properties of constituent particles. For example, numerical simulations by Wada et al. (2009) and Hasegawa et al. (2021) found that $v_{\text{fra}} \simeq 50\text{--}60 \text{ m s}^{-1}$ when the collision of two equal-mass dust aggregates made of $0.1 \text{ }\mu\text{m}$ -sized H_2O ice particles is considered.

The stickiness of dust particles has also been investigated in a huge number of studies (e.g., Poppe et al. 2000; Güttler et al. 2012; Tanaka et al. 2012; Krijt et al. 2013; Gundlach & Blum 2015; Nietiadi et al. 2017, 2020, 2022; Quadery et al.

2017; Arakawa & Krijt 2021). These studies found that the threshold velocity for the sticking in a head-on collision of individual dust particles is several times higher than that predicted for perfectly elastic spheres. Gundlach & Blum (2015) and Arakawa & Krijt (2021) concluded that the viscous dissipation would play a critical role in collision between micron-sized H₂O ice particles.

Nevertheless, impacts of viscous dissipation on the collisional behavior of dust aggregates have not been studied in detail. Most of numerical simulations of collisions between dust aggregates did not include the viscous dissipation force (e.g., Dominik & Tielens 1997; Wada et al. 2007, 2008, 2009; Hasegawa et al. 2021). Although a small number of studies (e.g., Seizinger et al. 2013; Umstätter & Urbassek 2021a,b) introduced the viscous dissipation force to their numerical simulations of collisions between dust aggregates, the dependence of v_{fra} on the strength of viscous dissipation force is still poorly understood. For head-on collisions between equal-mass dust aggregates, Umstätter & Urbassek (2021b) reported that the threshold velocity increases with increasing the strength of viscous dissipation force; however, when we consider oblique collisions, whether the viscous dissipation helps the collisional growth of dust aggregates is still unclear.

Here we report the results from numerical simulations of collisions between two equal-mass dust aggregates with various collision velocity and impact parameters. We also changed the strength of viscous dissipation force systematically. Surprisingly, we found that the threshold collision velocity for the fragmentation of dust aggregates hardly depends on the strength of viscous dissipation force when we consider oblique collisions. In contrast, the size distribution of fragments changes significantly when the viscous dissipation force is considered. We also obtained the empirical fitting formulae for the size distribution of fragments for the case of strong dissipation, which would be useful to study the evolution of size and spatial distributions of dust aggregates in protoplanetary disks.

2. MODEL

We performed three-dimensional numerical simulations of collisions between two equal-mass dust aggregates. The numerical code used in this study is based on the code developed by Wada et al. (2009), and we introduced the viscous drag term as Seizinger et al. (2013) considered.

2.1. Material parameters

In this study, we assume that dust particles constituting dust aggregates are made of water ice, and the all particles have the same radius of $r_1 = 0.1 \mu\text{m}$. The material parameters of water ice particles used in this study are listed in Table 1. These parameters are identical to that used in Wada et al. (2009) and Hasegawa et al. (2021).

Table 1. List of material parameters used in this study.

Parameter	Symbol	Value
Particle radius	r_1	0.1 μm
Material density	ρ	1000 kg m^{-3}
Surface energy	γ	100 mJ m^{-2}
Young's modulus	\mathcal{E}	7 GPa
Poisson's ratio	ν	0.25
Critical rolling displacement	ξ_{crit}	0.8 nm

2.2. Normal motion

Here we briefly describe the interparticle forces in the normal direction (for details, see Dominik & Tielens 1997; Wada et al. 2007). When two particles in contact are elastic spheres having a surface energy, their elastic behavior causes a repulsive force and the surface energy causes an attractive force. Johnson et al. (1971) formulated the particle interaction described below.

Two particles in contact make a contact area. At the equilibrium state, the contact radius, a , is equal to the equilibrium radius, a_0 , given by

$$a_0 = \frac{9\pi\gamma R^2}{\mathcal{E}^*}^{1/3}, \quad (1)$$

where $R = r_1/2$ is the reduced particle radius and $\mathcal{E}^* = \mathcal{E}/[2(1 - \nu^2)]$ is the reduced Young's modulus. The contact radius is related to the compression length between two particles in contact, δ , as follows:

$$\frac{\delta}{\delta_0} = 3 \frac{a}{a_0}^2 - 2 \frac{a}{a_0}^{1/2}, \quad (2)$$

where $\delta_0 = a_0^2/(3R)$ is the equilibrium compression length when $a = a_0$. Two particles in contact separate when compression length reaches $\delta = -\delta_c$, where

$$\delta_c = \frac{9}{16} \delta_0^{1/3}. \quad (3)$$

In this study, the normal force acting between two particles, F , is given by the sum of the two terms;

$$F = F_E + F_D, \quad (4)$$

where F_E is the force arising from the elastic deformation of particles and F_D is the force related to the viscous drag. The elastic force is given by Johnson et al. (1971) as

$$\frac{F_E}{F_c} = 4 \frac{a}{a_0}^3 - \frac{a}{a_0}^{3/2}, \quad (5)$$

where

$$F_c = 3\pi\gamma R, \quad (6)$$

is the maximum force needed to separate the two particles in contact. The viscous drag force is given by [Seizinger et al. \(2013\)](#) as follows;

$$F_D = \frac{2T_{\text{vis}}\mathcal{E}^*}{\nu^2}av_{\text{rel}}, \quad (7)$$

where v_{rel} is the normal component of the relative velocity of the two particles and T_{vis} is the viscoelastic timescale that is related to the strength of the viscous drag force (see also [Krijt et al. 2013](#)).

The value of T_{vis} for 0.1 μm -sized H_2O ice particles is not yet understood. Based on laboratory experiments ([Gundlach & Blum 2015](#); [Musiolik et al. 2016](#)), the threshold velocity for sticking in a head-on collision of individual micron-sized ice particle is approximately 10 times higher than that predicted from the theoretical model of [Johnson et al. \(1971\)](#). To reproduce the experimental results, [Gundlach & Blum \(2015\)](#) showed that $T_{\text{vis}} \simeq 10^{-10}$ s is plausible for $r_1 = 1.5 \mu\text{m}$, and [Arakawa & Krijt \(2021\)](#) also reported that $T_{\text{vis}} \simeq 10^{-8}$ s is plausible for $r_1 = 90 \mu\text{m}$. A simple extrapolation suggests that $T_{\text{vis}} \simeq 10^{-12}$ – 10^{-11} s for $r_1 = 0.1 \mu\text{m}$. We note that T_{vis} should depend not only on the particle radius but also on their temperature and the size of crystal domains in reality. Future studies on the strength of the viscous drag force using molecular dynamics simulations and laboratory experiments are essential.

The potential energy for normal motion of the two particles in contact, U_n , is given by

$$\frac{U_n}{F_c\delta_c} = 4 \times 6^{1/3} \times \frac{4}{5} \frac{a}{a_0} - \frac{4}{3} \frac{a}{a_0} + \frac{1}{3} \frac{a}{a_0} \quad (8)$$

When two particles collide, the compression length is $\delta = 0$ and the potential energy for normal motion of the newly formed contact is

$$U_n(0) = -\frac{8}{15} \times 2^{2/3} F_c \delta_c, \quad (9)$$

and the energy of $-U_n(0)$ dissipates due to connection. Similarly, when two particles separate, the compression length is $\delta = -\delta_c$ and the potential energy for normal motion before the disconnection is

$$U_n(-\delta_c) = \frac{4}{45} F_c \delta_c, \quad (10)$$

and the energy of $U_n(-\delta_c)$ dissipates due to disconnection. In addition, the potential energies stored by tangential displacement also dissipate when two particles separate (see Section 2.3). The potential energy at the equilibrium state ($\delta = \delta_0$) is

$$U_n(\delta_0) = -\frac{4}{5} \times 6^{1/3} F_c \delta_c. \quad (11)$$

Therefore, the energy needed to break a contact in the equilibrium by quasistatic process ($v_{\text{rel}} \rightarrow 0$ and $F_D \rightarrow 0$), E_{break} , is given by

$$E_{\text{break}} = U_n(-\delta_c) - U_n(\delta_0) = 6.1 \times 10^{-17} \text{ J}. \quad (12)$$

2.3. Tangential motion

The tangential motion of two particles in contact is divided into three motions: rolling, sliding, and twisting. The displacements corresponding to these motions are described as the rotation of two particles in contact. [Wada et al. \(2007\)](#) described the particle interaction models for these tangential motions (see also [Dominik & Tielens 1995, 1996](#)). Based on the framework of [Wada et al. \(2007\)](#), tangential motions of particles in contact are described by the linear spring model with critical displacements to their elastic limits. Here we briefly explain the outline.

2.3.1. Rolling motion

The potential energy stored by the rolling displacement is

$$U_r = \frac{1}{2} k_r \xi^2, \quad (13)$$

where ξ is the length of the rolling displacement and k_r is the spring constant that is given by

$$k_r = \frac{4F_c}{R}. \quad (14)$$

The critical rolling displacement is set to be $\xi_{\text{crit}} = 0.8 \text{ nm}$.¹ The critical energy required to start rolling, $E_{r,\text{crit}}$, is given by

$$E_{r,\text{crit}} = \frac{1}{2} k_r \xi_{\text{crit}}^2 = 1.2 \times 10^{-18} \text{ J}. \quad (15)$$

[Wada et al. \(2007\)](#) introduced E_{roll} as the energy needed to rotate a particle by $\pi/2$ radian around its contact point (see also [Dominik & Tielens 1997](#)). For the case of water ice particles of $r_1 = 0.1 \mu\text{m}$, E_{roll} is given by

$$E_{\text{roll}} = k_r \xi_{\text{crit}} \pi R = 4.7 \times 10^{-16} \text{ J}. \quad (16)$$

2.3.2. Sliding motion

¹ We note that ξ_{crit} represents the adhesion hysteresis of the contact area, and ξ_{crit} may depend on the crack velocity (see [Krijt et al. 2014](#), and references therein). Although we do not consider the viscoelastic model for the adhesion hysteresis of the contact area (e.g., [Arakawa & Krijt 2021](#)) for simplicity, future studies on this point would be interesting.

The potential energy stored by the sliding displacement is

$$U_s = \frac{1}{2}k_s\zeta^2, \quad (17)$$

where ζ is the length of the sliding displacement and k_s is the spring constant that is given by

$$k_s = 8a_0\mathcal{G}^*, \quad (18)$$

where $\mathcal{G}^* = \mathcal{G}/[2(2-\nu)]$. The shear modulus, \mathcal{G} , is related to the Young's modulus and the Poisson's ratio as $\mathcal{G} = \mathcal{E}/[2(1+\nu)]$. The critical sliding displacement, ζ_{crit} , is

$$\zeta_{\text{crit}} = \frac{2-\nu}{16\pi}a_0. \quad (19)$$

The critical energy required to start sliding, $E_{s,\text{crit}}$, is given by

$$\begin{aligned} E_{s,\text{crit}} &= \frac{1}{2}k_s\zeta_{\text{crit}}^2 \\ &= 7.3 \times 10^{-18} \text{ J}, \end{aligned} \quad (20)$$

and the energy needed to slide a particle by $\pi/2$ radian around its contact point, E_{slide} , is given by

$$\begin{aligned} E_{\text{slide}} &= k_s\zeta_{\text{crit}}\pi R \\ &= 1.7 \times 10^{-14} \text{ J}. \end{aligned} \quad (21)$$

2.3.3. Twisting motion

The potential energy stored at a twisting angle ϕ is

$$U_t = \frac{1}{2}k_t\phi^2, \quad (22)$$

and the spring constant k_t is given by

$$k_t = \frac{16}{3}\mathcal{G}'a_0^3, \quad (23)$$

where $\mathcal{G}' = \mathcal{G}/2$ is the reduced shear modulus. The critical angle for twisting, ϕ_{crit} , is

$$\phi_{\text{crit}} = \frac{1}{16\pi}. \quad (24)$$

The critical energy required to start twisting, $E_{t,\text{crit}}$, is given by

$$\begin{aligned} E_{t,\text{crit}} &= \frac{1}{2}k_t\phi_{\text{crit}}^2 \\ &= 2.8 \times 10^{-18} \text{ J}, \end{aligned} \quad (25)$$

and the energy needed to twist over $\pi/2$ radian is given by

$$\begin{aligned} E_{\text{twist}} &= k_t\phi_{\text{crit}}\frac{\pi}{2} \\ &= 4.4 \times 10^{-16} \text{ J}. \end{aligned} \quad (26)$$

In our numerical simulations, the energy is normalized by $F_c\delta_c = 4.0 \times 10^{-17} \text{ J}$. The particle interaction energies for both normal and tangential motions are listed in Table 2.

Table 2. List of particle interaction energies.

Symbol	Value	Equation
$F_c\delta_c$	$4.0 \times 10^{-17} \text{ J}$	Eqs. (3) and (6)
E_{break}	$6.1 \times 10^{-17} \text{ J}$	Eq. (12)
$E_{r,\text{crit}}$	$1.2 \times 10^{-18} \text{ J}$	Eq. (15)
E_{roll}	$4.7 \times 10^{-16} \text{ J}$	Eq. (16)
$E_{s,\text{crit}}$	$7.3 \times 10^{-18} \text{ J}$	Eq. (20)
E_{slide}	$1.7 \times 10^{-14} \text{ J}$	Eq. (21)
$E_{t,\text{crit}}$	$2.8 \times 10^{-18} \text{ J}$	Eq. (25)
E_{twist}	$4.4 \times 10^{-16} \text{ J}$	Eq. (26)

2.4. Initial condition

As the initial condition, we prepare two dust aggregates before collisions by ballistic particle–cluster aggregation (BPCA), i.e., sequential hit-and-stick collisions between a cluster (aggregate) and multiple single particles (e.g., Mukai et al. 1992). In this study, we set the number of particles constituting the target aggregate, N_{tar} , is equal to that for the projectile aggregate, N_{pro} , and both N_{tar} and N_{pro} are set to be 50,000. The total number of particles in a simulation, $N_{\text{tot}} = N_{\text{tar}} + N_{\text{pro}}$, is therefore 100,000.

Offset collisions of two dust aggregates is described by the impact parameter, b_{off} . The maximum impact parameter, b_{max} , is the sum of the radii of target and projectile aggregates; $b_{\text{max}} = r_{c,\text{tar}} + r_{c,\text{pro}}$. The radii of dust aggregates are calculated by the characteristic radius, r_c , which is given by $r_c = \sqrt{5/3}r_{\text{gyr}}$, and r_{gyr} is the gyration radius (Mukai et al. 1992). The radii of two dust aggregates used in this study are $r_{c,\text{tar}} = 72.29r_1$ and $r_{c,\text{pro}} = 72.25r_1$. Hereafter we use the normalized impact parameter, B_{off} , which is defined as

$$B_{\text{off}} \equiv \frac{b_{\text{off}}}{b_{\text{max}}}. \quad (27)$$

The square of the normalized impact parameter ranges from $B_{\text{off}}^2 = 0$ to 1 with an interval of $1/12$. The collision velocity of two dust aggregates, v_{col} , is set to $10^{(0.1i)} \text{ m s}^{-1}$, where $i = 13, 14, \dots, 20$. We also change T_{vis} that controls the strength of the viscous dissipation. We set $T_{\text{vis}} = 0 \text{ ps}$, 1 ps , 3 ps , and 6 ps ($1 \text{ ps} = 10^{-12} \text{ s}$). Therefore we carried out 416 ($= 13 \times 8 \times 4$) runs in this study.

3. RESULTS

3.1. Examples of collisional outcomes

Figure 1 shows the snapshots of collisional outcomes. Here we show the results for the cases of $v_{\text{col}} = 50.1 \text{ m s}^{-1}$ and $B_{\text{off}}^2 = 3/12$. We found that the collisional behavior is similar among different settings of the viscous dissipation when we focus on large fragments (panels (e)–(h)). In addition, the number of constituent particles in the largest fragment, N_{lar} , hardly depends on T_{vis} : $N_{\text{lar}} = 43957$ for $T_{\text{vis}} = 0 \text{ ps}$, $N_{\text{lar}} = 44927$ for $T_{\text{vis}} = 1 \text{ ps}$, $N_{\text{lar}} = 46263$

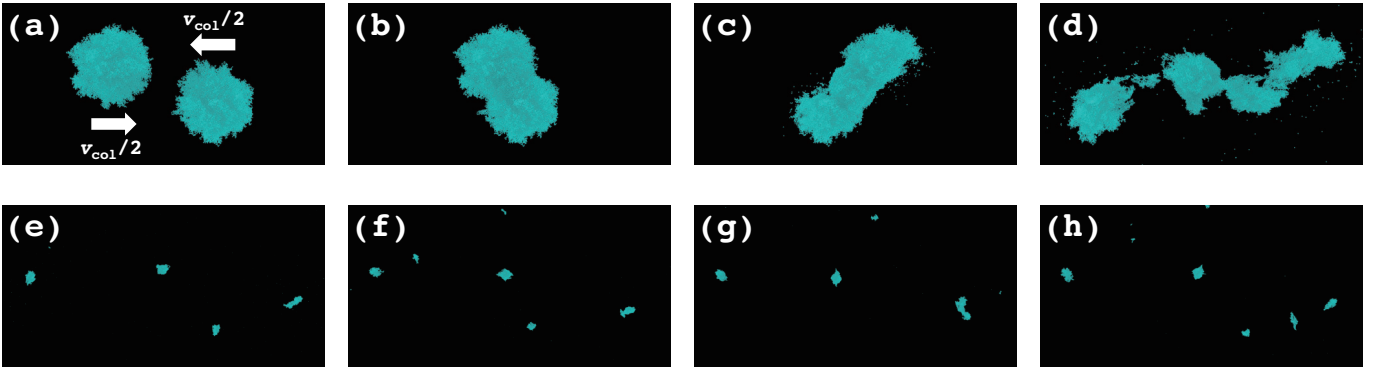


Figure 1. Snapshots of collisional outcomes. Here we set $v_{\text{col}} = 50.1 \text{ m s}^{-1}$ and $B_{\text{off}}^2 = 3/12$. Panels (a)–(d) are snapshots for $T_{\text{vis}} = 0 \text{ ps}$ (at $t = 0 \text{ } \mu\text{s}$, $0.32 \text{ } \mu\text{s}$, $0.63 \text{ } \mu\text{s}$, and $1.27 \text{ } \mu\text{s}$, respectively). Panels (e)–(h) are snapshots at $t = 6.34 \text{ } \mu\text{s}$ (for $T_{\text{vis}} = 0 \text{ ps}$, 1 ps , 3 ps , and 6 ps , respectively).

for $T_{\text{vis}} = 3 \text{ ps}$, and $N_{\text{lar}} = 47919$ for $T_{\text{vis}} = 6 \text{ ps}$. The amount of small fragments, however, strongly depends on T_{vis} . A large number of small fragments composed of one or two particle(s) are shown in Figures 1(c) and 1(d). In contrast, the number of small fragments significantly decreases when we non-zero T_{vis} is considered. In the following part of this section, we discuss the effects of the viscous dissipation on the collisional behavior of dust aggregates quantitatively.

3.2. Growth efficiency

First, we discuss the parameter dependence of the largest fragment formed after a collision. Here we introduce the collisional growth efficiency, f_{gro} , which is defined by Wada et al. (2013) as follows:

$$f_{\text{gro}} \equiv \frac{N_{\text{lar}} - N_{\text{tar}}}{N_{\text{pro}}}. \quad (28)$$

Figure 2 shows the collisional growth efficiency. In the range of $20 \text{ m s}^{-1} < v_{\text{col}} < 100 \text{ m s}^{-1}$, $f_{\text{gro}} \simeq 1$ for the cases of head-on collisions (i.e., $B_{\text{off}} = 0$). In contrast, we found that f_{gro} is negative for several cases with non-zero B_{off} . We can observe these trends in both zero and non-zero T_{vis} cases as shown in Figure 2.

When we consider the collisions between dust aggregates in protoplanetary disks, the impact parameter varies with each collision event. Then the average value of f_{gro} weighted over B_{off} would be the measure to investigating the dust growth in protoplanetary disks. The average value of a variable A weighted over B_{off} is given by

$$\langle A \rangle \equiv \frac{1}{\pi} \int_0^1 dB_{\text{off}} 2\pi B_{\text{off}} A(B_{\text{off}}). \quad (29)$$

The gray lines in Figure 2 shows the B_{off} -weighted average of f_{gro} , i.e., $\langle f_{\text{gro}} \rangle$. As $\langle f_{\text{gro}} \rangle$ decreases with increasing v_{col} , we can calculate the threshold collision velocity for the fragmentation of dust aggregates, v_{fra} , which is defined as the velocity where $\langle f_{\text{gro}} \rangle = 0$.

Figure 3 shows $\langle f_{\text{gro}} \rangle$ as a function of v_{col} . We found that $\langle f_{\text{gro}} \rangle$ hardly depends on the strength of the viscous dissipation, T_{vis} . For all cases of T_{vis} , $\langle f_{\text{gro}} \rangle$ is positive for $v_{\text{col}} < 50 \text{ m s}^{-1}$ and is negative for $v_{\text{col}} > 60 \text{ m s}^{-1}$. Therefore $v_{\text{fra}} \simeq 50\text{--}60 \text{ m s}^{-1}$ is obtained from our numerical simulations; this value is in good agreement with that obtained from previous studies (Wada et al. 2009; Hasegawa et al. 2021).

We note that f_{gro} for head-on collisions strongly depends on T_{vis} as Umstätter & Urbassek (2021b) reported. Figure 4 shows f_{gro} for high-speed head-on collisions. We confirmed that the threshold velocity for collisional growth/fragmentation for head-on collisions increases with T_{vis} , although $\langle f_{\text{gro}} \rangle$ should be considered for the dust growth in protoplanetary disks.

3.3. Threshold velocity for growth/fragmentation

The threshold velocity for sticking in a head-on collision of individual dust particle, v_{stick} , is a function of T_{vis} .² For a head-on collision of identical particles, the equation of motion is given by

$$\ddot{\delta} = -\frac{F}{m^*}, \quad (30)$$

where $m^* = m_1/2$ is the reduced mass, and $m_1 = (4\pi/3)\rho r_1^3$ is the mass of each particle. The normal force acting between two particles, F , is given by Eq. (4), and we integrated Eq. (30) for different settings of T_{vis} and v_{col} . Then we obtained the threshold velocity for sticking as a function of T_{vis} .

Figure 5 shows v_{stick} and v_{fra} as functions of T_{vis} . Although v_{stick} for $T_{\text{vis}} = 6 \text{ ps}$ is approximately 10 times higher than that for $T_{\text{vis}} = 0 \text{ ps}$, v_{fra} hardly depends on

² When we consider a head-on collision of two individual dust particles without fragmentation/evaporation/melting, the collisional outcomes are classified into two cases: sticking (i.e., $f_{\text{gro}} = 1$) and bouncing (i.e., $f_{\text{gro}} = 0$). The collisional outcome is sticking when $v_{\text{col}} \leq v_{\text{stick}}$, and bouncing occurs if $v_{\text{col}} > v_{\text{stick}}$.

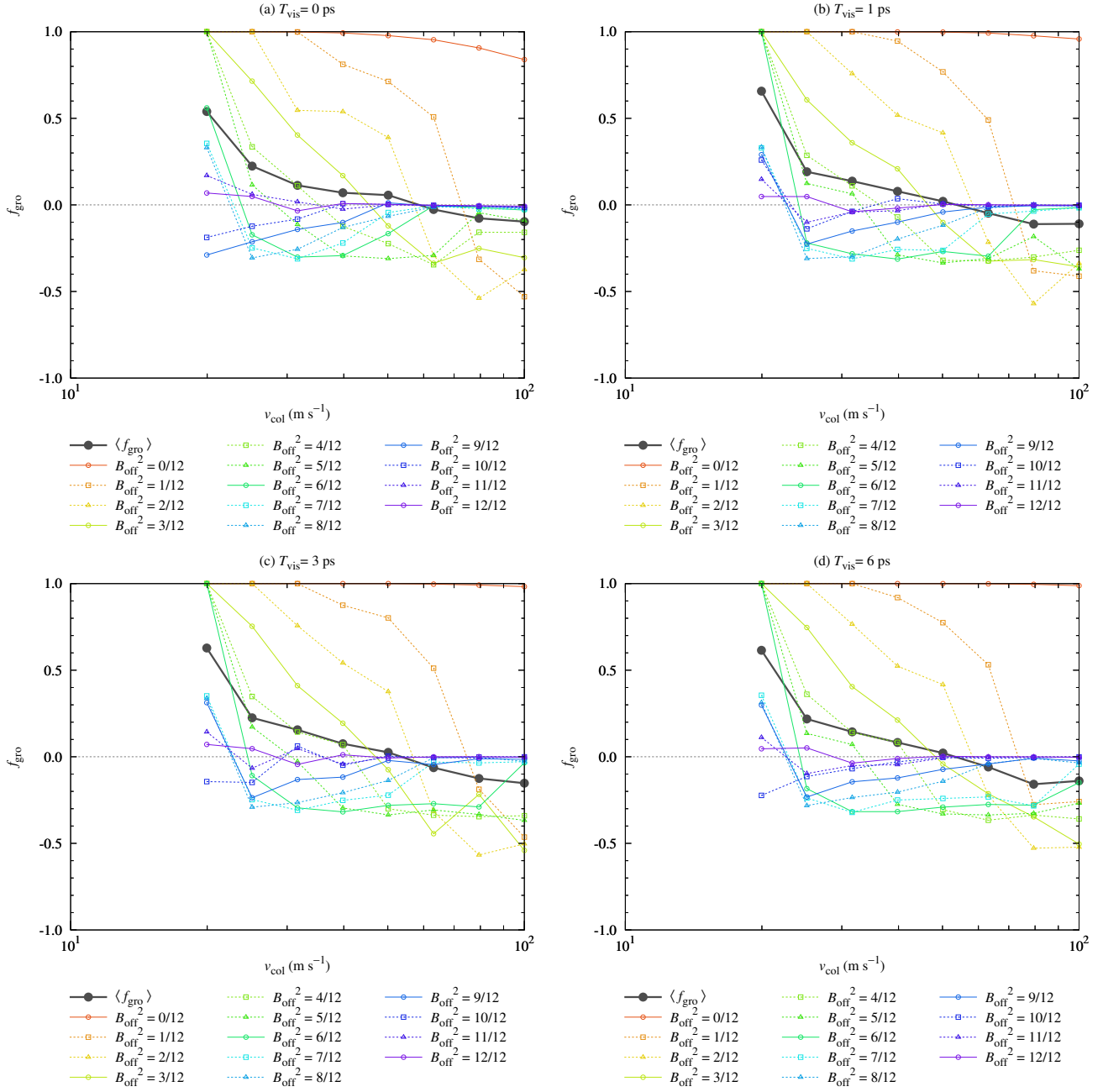


Figure 2. Collisional growth efficiency, f_{gro} , for different settings of T_{vis} , B_{off} , and v_{col} .

T_{vis} . This indicates that the dominant energy dissipation process for collisions of dust aggregates is different from that for head-on collisions of individual particles.

3.4. Size distribution of fragments

Second, we report the size distribution of fragments formed after collisions. We define $n(N)$ as the number of fragments that consist of N particles. The cumulative number of fragments that contain not smaller than N particles,

$Z_{\text{cum}}(\geq N)$, is defined as follows:

$$Z_{\text{cum}}(\geq N) \equiv \sum_{N'=\lceil N \rceil}^{\mathcal{N}_{\text{ot}}} n(N'), \quad (31)$$

where $\lceil N \rceil$ is the smallest integer that is not smaller than N . Figure 6 shows the B_{off} -weighted average of $Z_{\text{cum}}(\geq N)$ for the cases of $v_{\text{col}} = 50.1 \text{ m s}^{-1}$ and 100 m s^{-1} . We found that $\langle Z_{\text{cum}}(\geq N) \rangle$ strongly depends on T_{vis} for $N \lesssim 10$. In contrast, the dependence of $\langle Z_{\text{cum}}(\geq N) \rangle$ on T_{vis} is weak for $N \gg 10$. This is consistent with the fact that the collisional

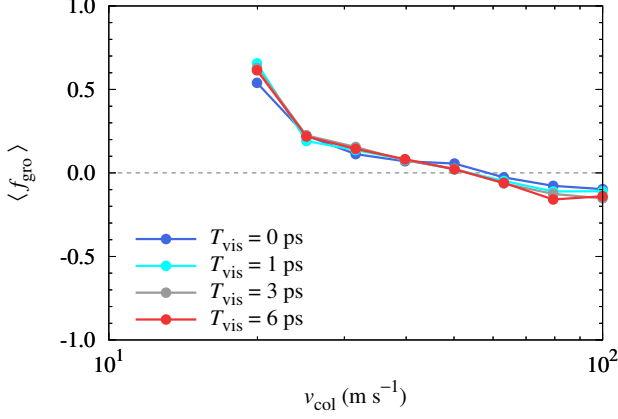


Figure 3. B_{off} -weighted collisional growth efficiency, $\langle f_{\text{gro}} \rangle$.

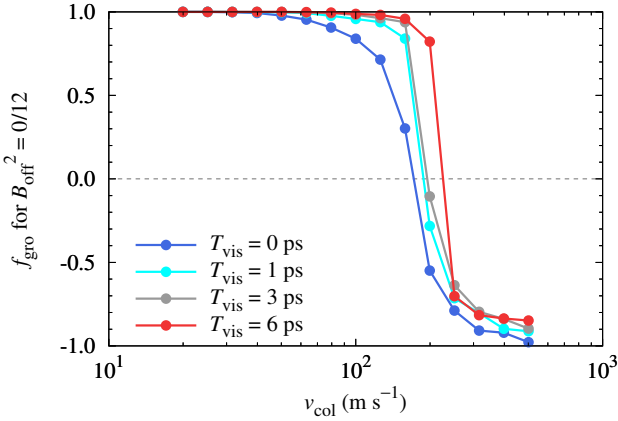


Figure 4. Collisional growth efficiency for high-speed head-on collisions.

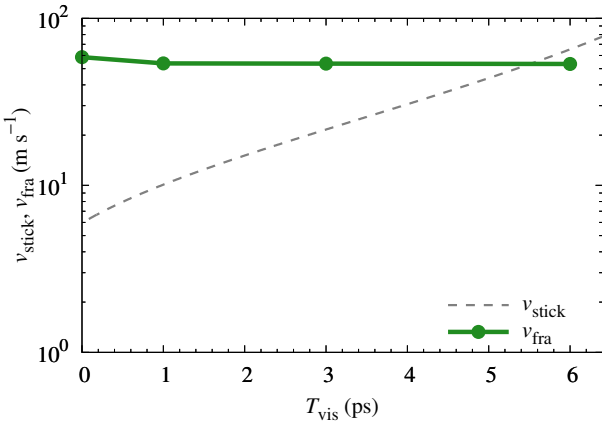


Figure 5. v_{stick} and v_{fra} as functions of T_{vis} .

behavior is similar among different settings of T_{vis} when we focus on large fragments (see Figure 1). We also note that $\langle Z_{\text{cum}}(\geq N) \rangle$ depends on v_{col} , especially for the cases of $T_{\text{vis}} = 0$ ps. This trend is consistent with the results of Wada et al. (2009).

The cumulative number of particles that are constituents of fragments that contain not larger than N particles, $N_{\text{cum}}(\leq N)$, is defined as follows:

$$N_{\text{cum}}(\leq N) \equiv \sum_{N'=1}^{\lfloor N \rfloor} n(N')N', \quad (32)$$

where $\lfloor N \rfloor$ is the largest integer that is not larger than N . Figure 7 shows the B_{off} -weighted average of $N_{\text{cum}}(\leq N)$ for the cases of $v_{\text{col}} = 50.1 \text{ m s}^{-1}$ and 100 m s^{-1} . As shown in Figure 7, largest fragments dominate the mass for the cases of both $v_{\text{col}} = 50.1 \text{ m s}^{-1}$ and 100 m s^{-1} . In addition, our numerical results indicate that $\langle N_{\text{cum}}(\leq N) \rangle$ is approximately proportional to N for $N \gg 10^2$ when we consider the non-zero T_{vis} . We provide an empirical fitting of $\langle N_{\text{cum}}(\leq N) \rangle$ in Section 4.

We evaluate the contribution to the geometric cross section. The geometric cross section of single particle, S_1 , is given by $S_1 = \pi r_1^2$. We define the equivalent geometric cross section of a fragment that consist of N particles, $S(N)$, as follows: $S(N) \equiv \pi r_1^2 N^{2/3}$. Then the cumulative of the geometric cross section of a fragment that contain not larger than N particles, $S_{\text{cum}}(\leq N)$, is given by

$$S_{\text{cum}}(\leq N) \equiv \sum_{N'=1}^{\lfloor N \rfloor} n(N')S(N'). \quad (33)$$

Figure 8 shows the B_{off} -weighted average of $S_{\text{cum}}(\leq N)$ for the cases of $v_{\text{col}} = 50.1 \text{ m s}^{-1}$ and 100 m s^{-1} . We found that $\langle S_{\text{cum}}(\leq N_{\text{tot}}) \rangle$ is dominated by largest fragments except for the case of $v_{\text{col}} = 100 \text{ m s}^{-1}$ and $T_{\text{vis}} = 0$ ps (blue line of Figure 8(b)).

4. EMPIRICAL FITTINGS FOR SIZE DISTRIBUTION OF FRAGMENTS

Figures 6–8 revealed that the size distribution of fragments strongly depends on the strength of viscous dissipation. When $T_{\text{vis}} = 6$ ps is assumed, we found that the size distribution of fragments at collision velocity of $v_{\text{col}} \sim v_{\text{fra}}$ is approximately fitted by simple curves as shown in Figure 9.

Here we assume that the number of fragments that contain not less than N and less than $N + \Delta N$ particles is given by $f(N)\Delta N$. Under this assumption, $\langle N_{\text{cum}}(N) \rangle$ is given by

$$\langle N_{\text{cum}}(\leq N) \rangle \simeq \int_0^N dN' f(N')N'. \quad (34)$$

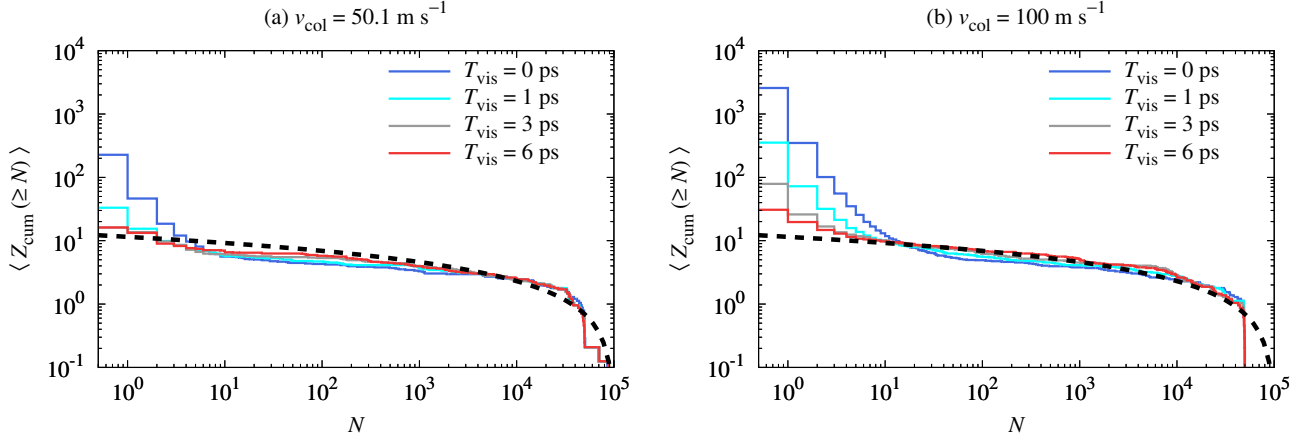


Figure 6. B_{off} -weighted average of $Z_{\text{cum}}(\geq N)$, $\langle Z_{\text{cum}}(\geq N) \rangle$. (a) For the case of $v_{\text{col}} = 50.1 \text{ m s}^{-1}$. (b) For the case of $v_{\text{col}} = 100 \text{ m s}^{-1}$. Black dashed lines are the empirical fittings (see Section 4).

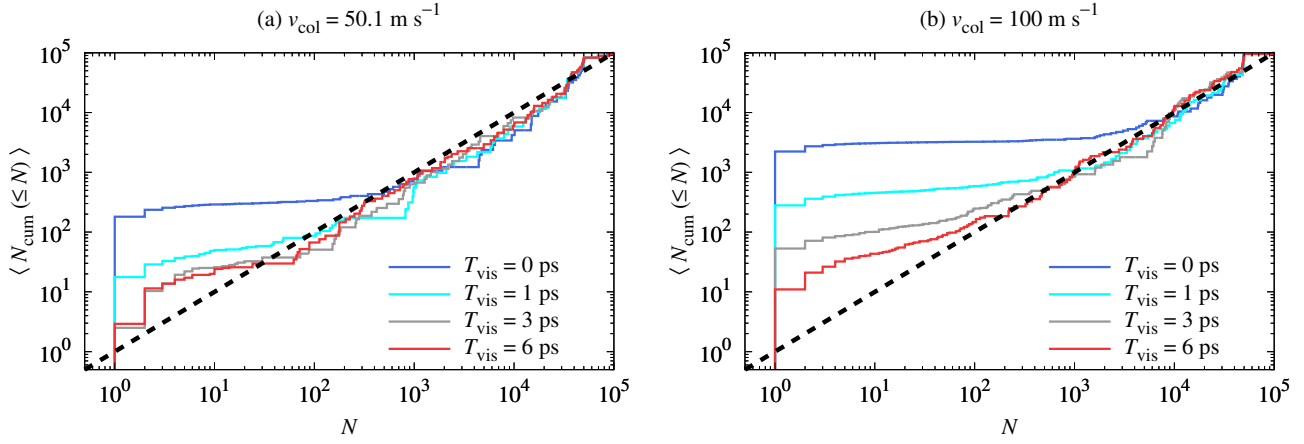


Figure 7. B_{off} -weighted average of $N_{\text{cum}}(\leq N)$, $\langle N_{\text{cum}}(\leq N) \rangle$. (a) For the case of $v_{\text{col}} = 50.1 \text{ m s}^{-1}$. (b) For the case of $v_{\text{col}} = 100 \text{ m s}^{-1}$. Black dashed lines are the empirical fittings (see Section 4).

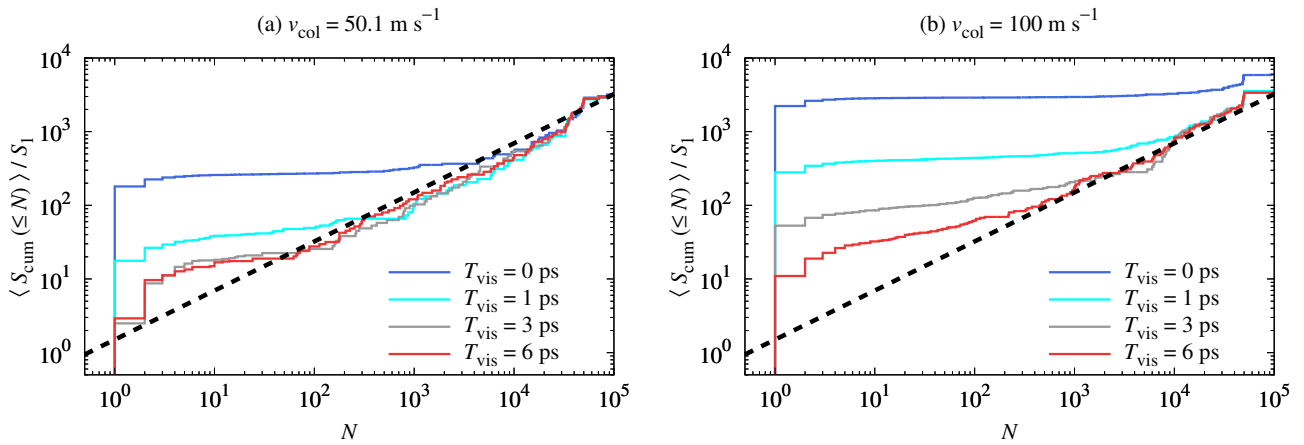


Figure 8. B_{off} -weighted average of $S_{\text{cum}}(\leq N)$, $\langle S_{\text{cum}}(\leq N) \rangle / S_1$. (a) For the case of $v_{\text{col}} = 50.1 \text{ m s}^{-1}$. (b) For the case of $v_{\text{col}} = 100 \text{ m s}^{-1}$. Black dashed lines are the empirical fittings (see Section 4).

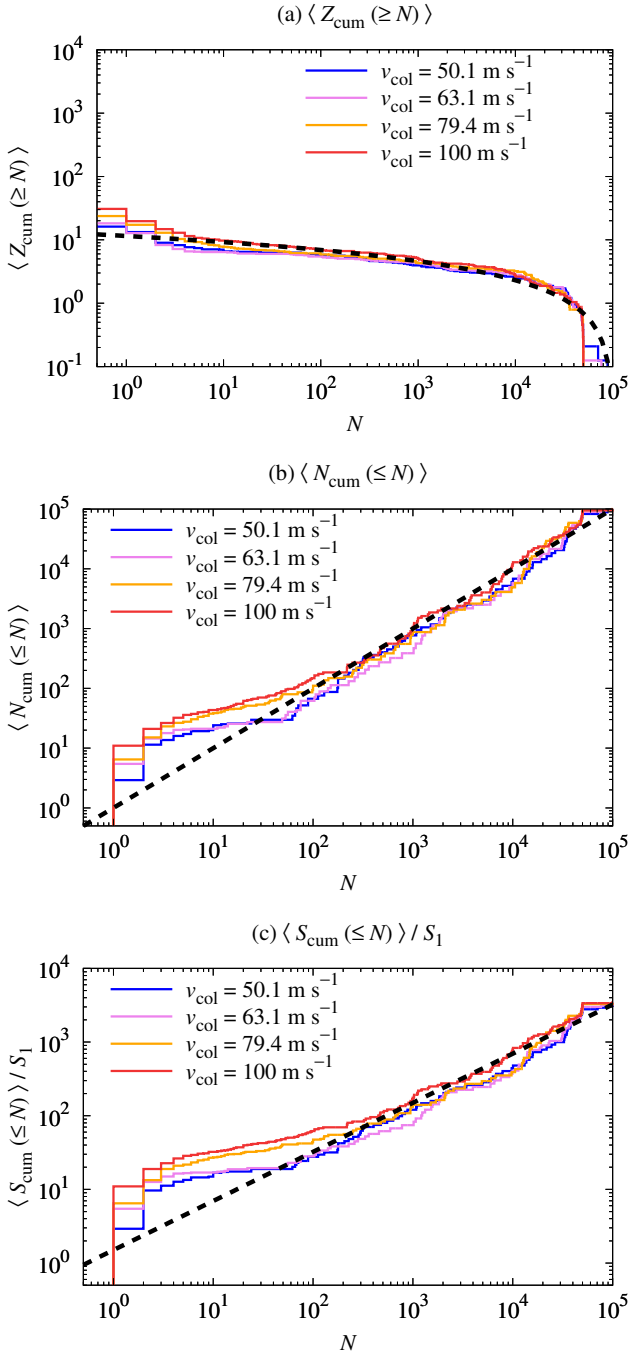


Figure 9. B_{off} -weighted average of size distributions of fragments. (a) $\langle Z_{\text{cum}}(\geq N) \rangle$. (b) $\langle N_{\text{cum}}(\leq N) \rangle$. (c) $\langle S_{\text{cum}}(\leq N) \rangle$. Black dashed lines are the empirical fittings. These size distributions are insensitive to v_{col} around v_{fra} .

For arbitrary N , the following relation,

$$\langle N_{\text{cum}}(\leq N) \rangle \simeq N, \quad (35)$$

reasonably reproduces the numerical results as shown in Figure 9(b). Combining Eqs. (34) and (35), we obtain the fol-

lowing equation:

$$f(N) \simeq \frac{1}{N}. \quad (36)$$

Using Eq. (36), $\langle Z_{\text{cum}}(\geq N) \rangle$ and $\langle S_{\text{cum}}(\leq N) \rangle$ are approximately given by

$$\begin{aligned} \langle Z_{\text{cum}}(\geq N) \rangle &\simeq \int_N^{N_{\text{tot}}} dN f(N) \\ &\simeq \log N_{\text{tot}} - \log N, \end{aligned} \quad (37)$$

and

$$\begin{aligned} \langle S_{\text{cum}}(\leq N) \rangle / S_1 &\simeq \int_0^N dN f(N) N^{2/3} \\ &\simeq \frac{3}{2} N^{2/3}, \end{aligned} \quad (38)$$

respectively. Black dashed lines in Figures 6–9 show the empirical fitting equations described above. These fittings are in agreement with numerical results. We note that the size distributions are insensitive to v_{col} around v_{fra} .

Here we briefly describe the generalized relations among $\langle Z_{\text{cum}}(\geq N) \rangle$, $\langle N_{\text{cum}}(\leq N) \rangle$, and $\langle S_{\text{cum}}(\leq N) \rangle$ as reference. For simplicity, we assume that $f(N)$ is given by a following power-law equation:

$$f(N) \simeq cN^{-\alpha} \quad (1 \leq N \leq N_{\text{tot}}), \quad (39)$$

where c and α are constants. Then $\langle Z_{\text{cum}}(\geq N) \rangle$, $\langle N_{\text{cum}}(\leq N) \rangle$, and $\langle S_{\text{cum}}(\leq N) \rangle$ are given as follows:

$$\begin{aligned} \langle Z_{\text{cum}}(\geq N) \rangle &\simeq \int_N^{N_{\text{tot}}} dN f(N) \\ &\simeq \begin{cases} cN_{\text{tot}}^{1-\alpha}/(1-\alpha) & (\alpha < 1), \\ c \log(N_{\text{tot}}/N) & (\alpha = 1), \\ cN^{1-\alpha}/(\alpha-1) & (\alpha > 1), \end{cases} \quad (40) \\ \langle N_{\text{cum}}(\leq N) \rangle &\simeq \int_0^N dN f(N) N \\ &\simeq \begin{cases} cN^{2-\alpha}/(2-\alpha) & (\alpha < 2), \\ c \log N & (\alpha = 2), \\ c/(\alpha-2) & (\alpha > 2), \end{cases} \quad (41) \end{aligned}$$

and

$$\begin{aligned} \frac{\langle S_{\text{cum}}(\leq N) \rangle}{S_1} &\simeq \int_0^N dN f(N) N^{2/3} \\ &\simeq \begin{cases} cN^{5/3-\alpha}/(5/3-\alpha) & (\alpha < 5/3), \\ c \log N & (\alpha = 5/3), \\ c/(\alpha-5/3) & (\alpha > 5/3), \end{cases} \quad (42) \end{aligned}$$

respectively. Therefore, largest fragments dominate the mass when $\alpha < 2$, and they also dominate the surface area when $\alpha < 5/3$ is satisfied. As our numerical results indicate that $\alpha \simeq 1$ for the case of non-zero T_{vis} , largest fragments dominate both mass and surface area.

We also note that size distributions of fragments produced by collisions of monolithic rocks (and ice) were studied in laboratory impact experiments. Mizutani et al. (1990) reviewed these experimental results, and they reported that the size distribution for smaller fragments is approximately given by a power-law with $\alpha \simeq 5/3$, although α weakly depends on the impact velocity and the material parameters. In addition, when we fit a power-law to the size distribution of larger fragments, α is larger than $5/3$ for catastrophic fragmentation and it strongly depends on the impact velocity and the material parameters. As α would be associated with the microphysics of fracture propagation, we should investigate what causes the relatively small α of dust aggregates compared with the case of monolithic rocks/ices in future studies.

5. DISCUSSION

In Section 3.3, we showed that v_{fra} is approximately independent of T_{vis} , although v_{stick} strongly depends on T_{vis} . In the following part, we perform the analyses of interparticle velocity and energy dissipation to understand the reason why v_{fra} is insensitive to T_{vis} .

5.1. Normal component of the interparticle velocity

Figure 10 shows the normal component of the interparticle velocity, v_{rel} , at $t = 0.32 \mu\text{s}$. Here we show the results with $v_{\text{col}} = 50.1 \text{ m s}^{-1}$ and $B_{\text{off}}^2 = 3/12$. We calculated v_{rel} for particle pairs whose interparticle distance is less than the threshold distance, $d_{\text{th}} = 2.2r_1$. We set the sign of v_{rel} is positive when two particles approach. Figure 11 also shows v_{rel} at $t = 0.63 \mu\text{s}$. We define $N_{\text{pair,p}}(> v_{\text{rel}})$ as the number of pairs whose interparticle velocity is higher than $v_{\text{rel}} > 0$, and $N_{\text{pair,n}}(< v_{\text{rel}})$ as the number of pairs whose interparticle velocity is lower than $v_{\text{rel}} < 0$.

We found that both $N_{\text{pair,p}}(> 10 \text{ m s}^{-1})$ and $N_{\text{pair,n}}(< -10 \text{ m s}^{-1})$ are less than 10^3 for all cases and are negligibly smaller than N_{tot} . This indicates that viscous energy dissipation, which is proportional to the square of v_{rel} , is not the main mechanism for the energy dissipation for collisions between dust aggregates.

The energy dissipation rate at a particle contact due to viscous dissipation force, \dot{E}_{vis} , is given by

$$\begin{aligned} \dot{E}_{\text{vis}} &= -F_{\text{D}}v_{\text{rel}} \\ &= 1.5 \times 10^{-9} \\ &\quad \times \frac{a}{a_0} \frac{T_{\text{vis}}}{1 \text{ ps}} \frac{v_{\text{rel}}}{1 \text{ m s}^{-1}}^2 \text{ J s}^{-1}. \end{aligned} \quad (43)$$

The kinetic energy per one particle with the velocity of $v_{\text{col}}/2$ is

$$\begin{aligned} E_{\text{kin},1} &= \frac{1}{2}m_1 \frac{v_{\text{col}}}{2}^2 \\ &= 1.3 \times 10^{-15} \frac{v_{\text{col}}}{50 \text{ m s}^{-1}}^2 \text{ J}. \end{aligned} \quad (44)$$

Figure 12 shows the temporal evolution of the root mean square of v_{rel} , $v_{\text{rel,rms}}$. For the cases with non-zero T_{vis} , we found that $v_{\text{rel,rms}}$ takes the maximum around $t \simeq 0.3 \mu\text{s}$ and the maximum value is lower than 1 m s^{-1} . In addition, $v_{\text{rel,rms}}$ decreases with the timescale of $\simeq 0.2 \mu\text{s}$ in these cases. As the total energy dissipation at a particle contact due to viscous dissipation force, E_{vis} , is given by the time integration of \dot{E}_{vis} , our results indicate that $E_{\text{vis}} < E_{\text{kin},1}$. In other words, the viscous energy dissipation would not be the main mechanism for the energy dissipation for collisions between dust aggregates.

5.2. Energy dissipation mechanisms

We check the total energy dissipation due to particle interactions from $t = 0$ and discuss which is the main mechanism for the energy dissipation. Figure 13 shows the temporal evolution of the total energy dissipation due to rolling friction ($E_{\text{dis,r}}$), sliding friction ($E_{\text{dis,s}}$), twisting friction ($E_{\text{dis,t}}$), connection and disconnection of particles ($E_{\text{dis,c}}$), and viscous drag force ($E_{\text{dis,v}}$). The particle interaction energies for interparticle motions are summarized in Table 2. Here we show the results with $v_{\text{col}} = 50.1 \text{ m s}^{-1}$ and $B_{\text{off}}^2 = 3/12$.

We found that the main mechanism for the energy dissipation is the rolling friction for all cases shown in Figure 13, and the energy dissipation due to connection and disconnection of particles is the smallest among five interaction mechanisms (except for the case of $T_{\text{vis}} = 0 \text{ ps}$, which results in $E_{\text{dis,v}} = 0$). The strength of the energy dissipation due to the viscous drag force increases with increasing T_{vis} (Figure 13(e)). On the other hand, the strength of the energy dissipation due to the sliding friction decreases with increasing T_{vis} (Figure 13(b)). The strength of the energy dissipation due to the twisting friction hardly depends on T_{vis} in this setting (Figure 13(c)). We will further investigate the physical origin of these trends in future studies.

Figure 14 shows the total energy dissipation due to particle interactions at the end of simulations ($E_{\text{dis,r}}$, $E_{\text{dis,s}}$, $E_{\text{dis,t}}$, $E_{\text{dis,c}}$, and $E_{\text{dis,v}}$). We set $B_{\text{off}}^2 = 3/12$ and investigated the dependence of the total energy dissipation on T_{vis} and v_{col} . We found that $E_{\text{dis,s}}$ strongly depends on v_{col} for all settings of T_{vis} (see Figure 14(b)), and $E_{\text{dis,s}}$ is not the main mechanism for the energy dissipation when $v_{\text{col}} \lesssim v_{\text{fra}}$. This strong dependence of $E_{\text{dis,s}}$ on v_{col} might be originated from the magnitude relation between E_{slide} and $E_{\text{kin},1}$ (see Table 2). When $v_{\text{col}} \lesssim v_{\text{fra}}$, the magnitude relation is $E_{\text{slide}} \gg E_{\text{kin},1}$ and the kinetic energy of colliding aggregates would not be

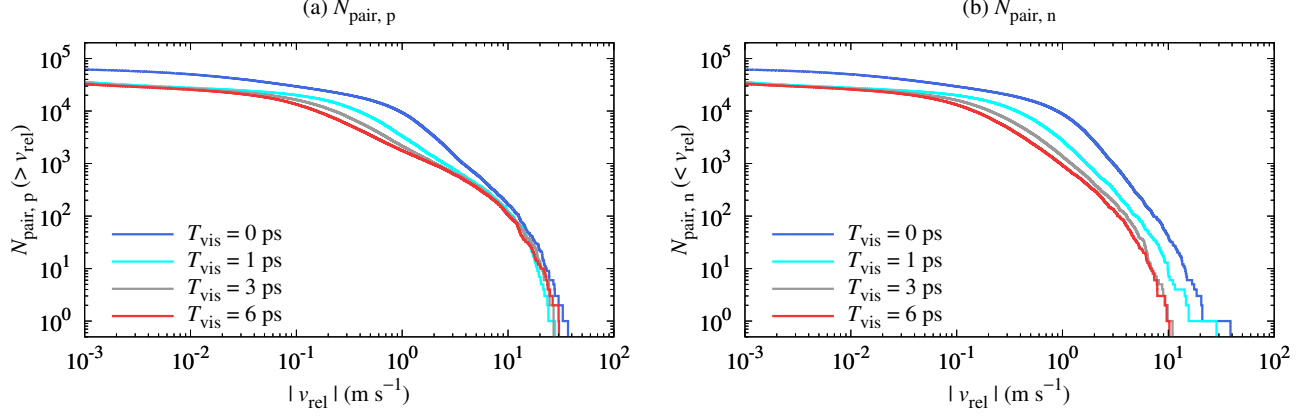


Figure 10. Cumulative frequencies of the normal component of the interparticle velocity, $N_{\text{pair},p}(>v_{\text{rel}})$ and $N_{\text{pair},n}(<v_{\text{rel}})$, at $t = 0.32 \mu\text{s}$. Here we show the results with $v_{\text{col}} = 50.1 \text{ m s}^{-1}$ and $B_{\text{off}}^2 = 3/12$.

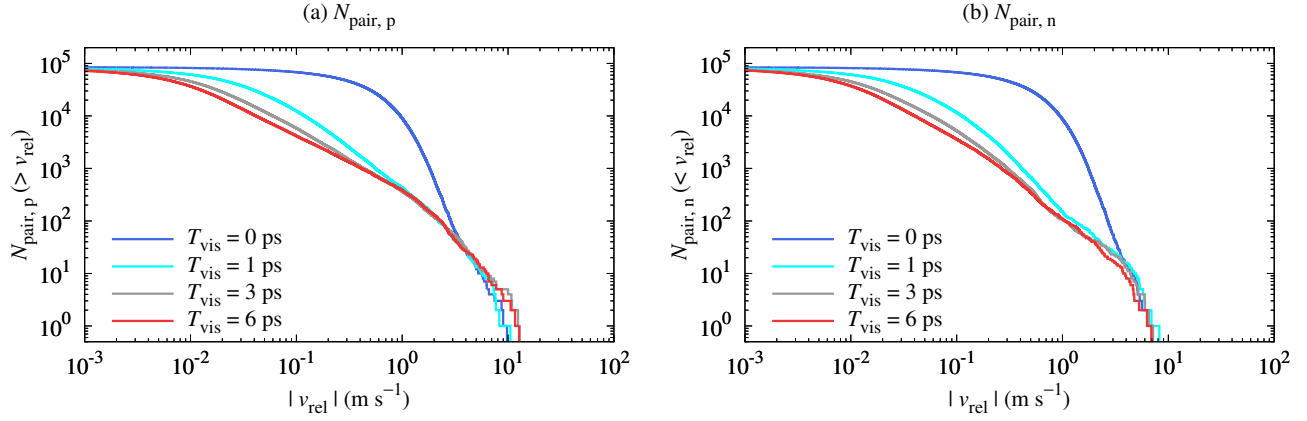


Figure 11. Cumulative frequencies of the normal component of the interparticle velocity, $N_{\text{pair},p}(>v_{\text{rel}})$ and $N_{\text{pair},n}(<v_{\text{rel}})$, at $t = 0.63 \mu\text{s}$.

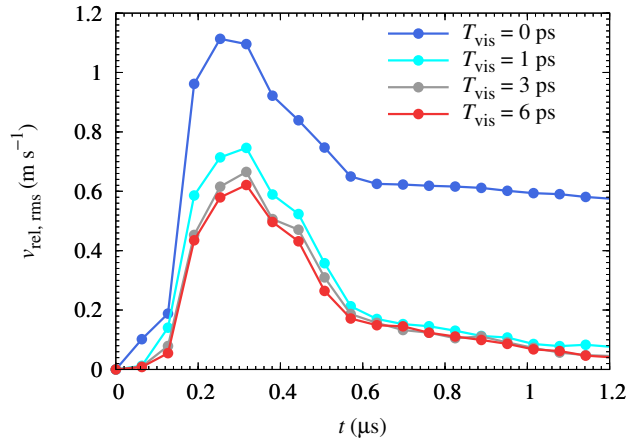


Figure 12. Temporal evolution of the root mean square of v_{rel} , $v_{\text{rel},\text{rms}}$. Here we show the results with $v_{\text{col}} = 50.1 \text{ m s}^{-1}$ and $B_{\text{off}}^2 = 3/12$.

enough to cause large sliding displacement. In contrast, when

$v_{\text{col}} \gtrsim 100 \text{ m s}^{-1}$, the condition $E_{\text{slide}} \gtrsim E_{\text{kin},1}$ is achieved and large sliding displacement could take place. We will test this hypothesis by systematically changing k_s in future studies.

The main mechanism for the energy dissipation is $E_{\text{dis},r}$ when the collision velocity is $v_{\text{col}} \lesssim v_{\text{fra}}$. We also found that $E_{\text{dis},c}/(N_{\text{tot}}F_c\delta_c)$ is on the order of 1 when $v_{\text{col}} \sim v_{\text{fra}}$ and this is common feature for all cases of T_{vis} (see Figure 14(d)). This is consistent with the fact that the sum of the number of connection and disconnection events is approximately equal to the total number of particles; $N_{\text{con}} + N_{\text{cut}} \simeq N_{\text{tot}}$ (see Section 5.3).

We note that [Dominik & Tielens \(1997\)](#) also described the trend for the magnitude relationship of energy dissipation mechanisms. Although they performed head-on collisions of equal-mass aggregates in two-dimensional space, the trend is similar to our results; the main mechanism for the energy dissipation is rolling for low-speed collisions, and sliding be-

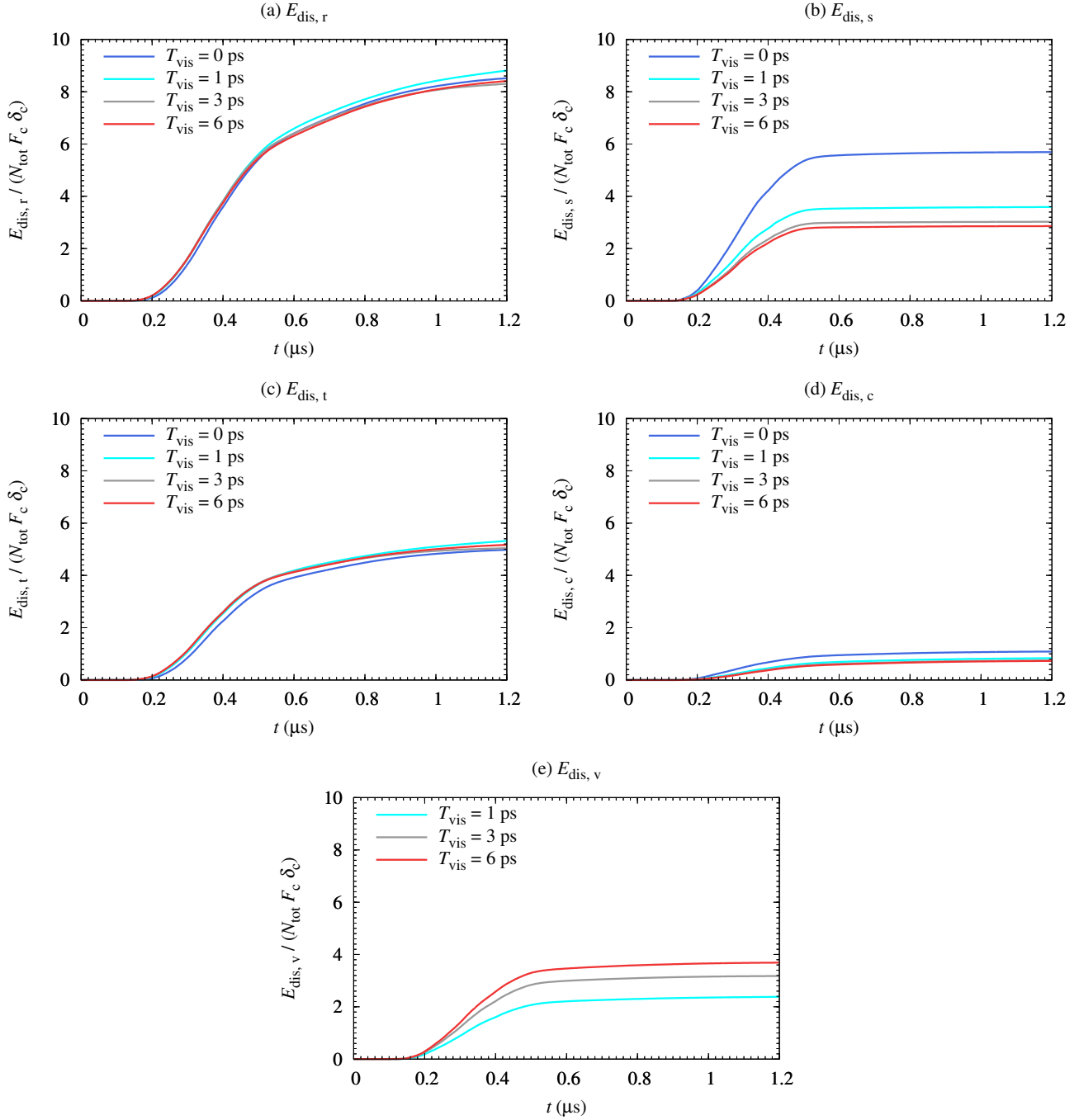


Figure 13. Temporal evolution of the total energy dissipation due to rolling friction ($E_{\text{dis},r}$), sliding friction ($E_{\text{dis},s}$), twisting friction ($E_{\text{dis},t}$), connection and disconnection of particles ($E_{\text{dis},c}$), and viscous drag force ($E_{\text{dis},v}$).

comes important when v_{col} is large. We confirmed this trend for head-on collisions in our three-dimensional simulations.

5.3. Particle connection and disconnection

Figure 15 shows the number of connection events, N_{con} , and disconnection events, N_{cut} , in a collision between dust aggregates with $B_{\text{off}}^2 = 3/12$. We found that both N_{con} and N_{cut} increases with decreasing T_{vis} and increasing v_{col} .

When we focus on the collision behavior around $v_{\text{col}} \simeq v_{\text{fra}}$, our numerical simulations revealed that $N_{\text{con}} \simeq N_{\text{tot}}$ and $N_{\text{cut}} < N_{\text{tot}}$ for all cases. This is in agreement with the results shown in Figure 14.

Wada et al. (2009) reported that each particle experiences multiple ($\gg 1$) events of connection and disconnection on average in a head-on collision of dust aggregates (see their Figure 5). Our results, in contrast, revealed that the aver-

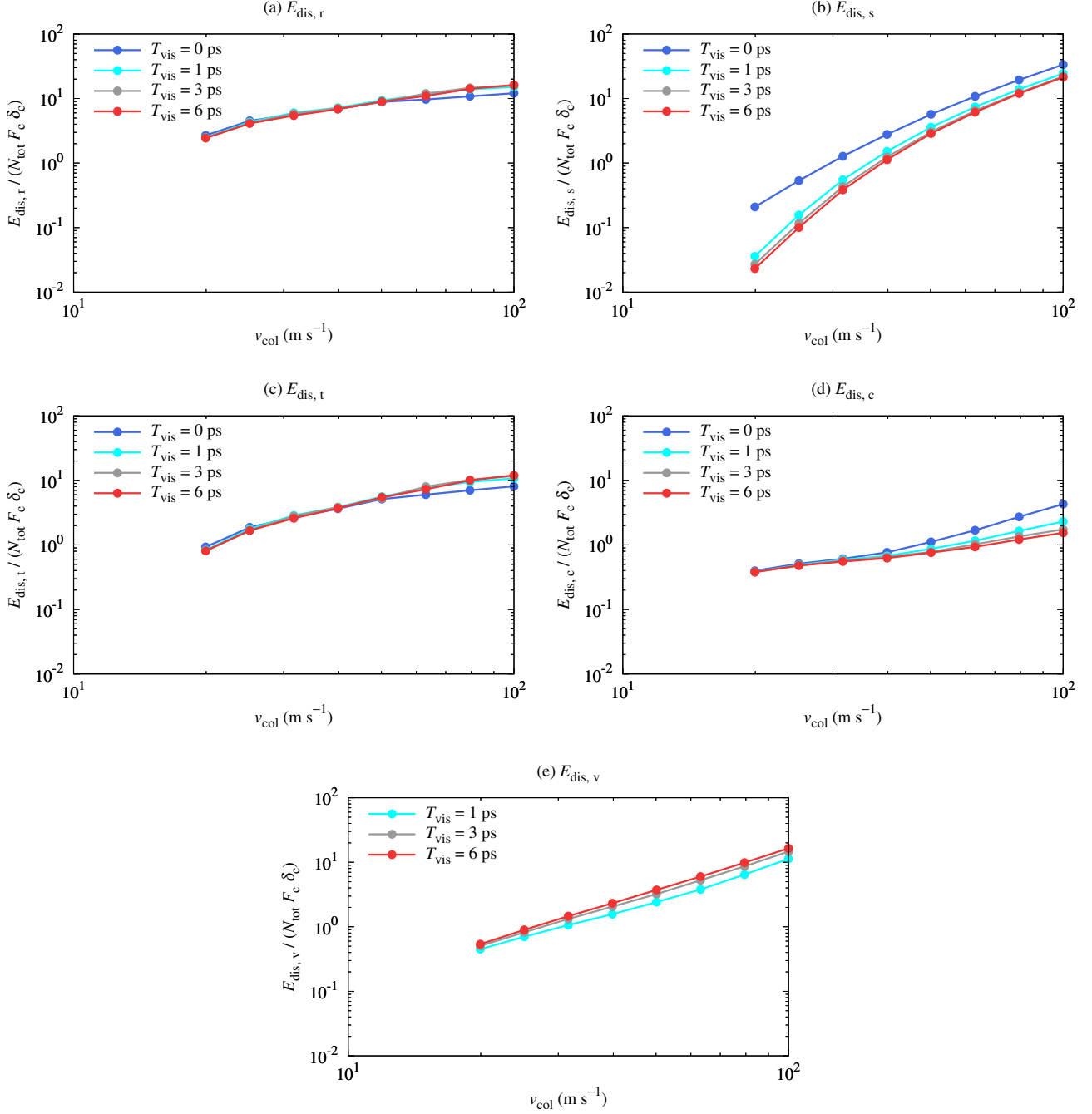


Figure 14. Total energy dissipation due to particle interactions at the end of simulations: (a) $E_{\text{dis},r}$, (b) $E_{\text{dis},s}$, (c) $E_{\text{dis},t}$, (d) $E_{\text{dis},c}$, and (e) $E_{\text{dis},v}$.

age number of events per a particle is approximately one (or a few) in a grazing collision, even if the normalized impact parameter is small ($B_{\text{off}}^2 = 3/12$). This would be related to the apparent discrepancy between our results and the results of Umstätter & Urbassek (2021b), who reported that the threshold velocity for collisional growth/fragmentation increases with the strength of viscous dissipation force for head-on collisions of dust aggregates.

6. SUMMARY

Understanding the collisional behavior of dust aggregates consisting of submicron-sized grains is essential to unveiling how planetesimals form in protoplanetary disks. It is known that the collisional behavior of individual dust particles strongly depends on the strength of viscous dissipation force (e.g., Gundlach & Blum 2015; Arakawa & Krijt 2021);

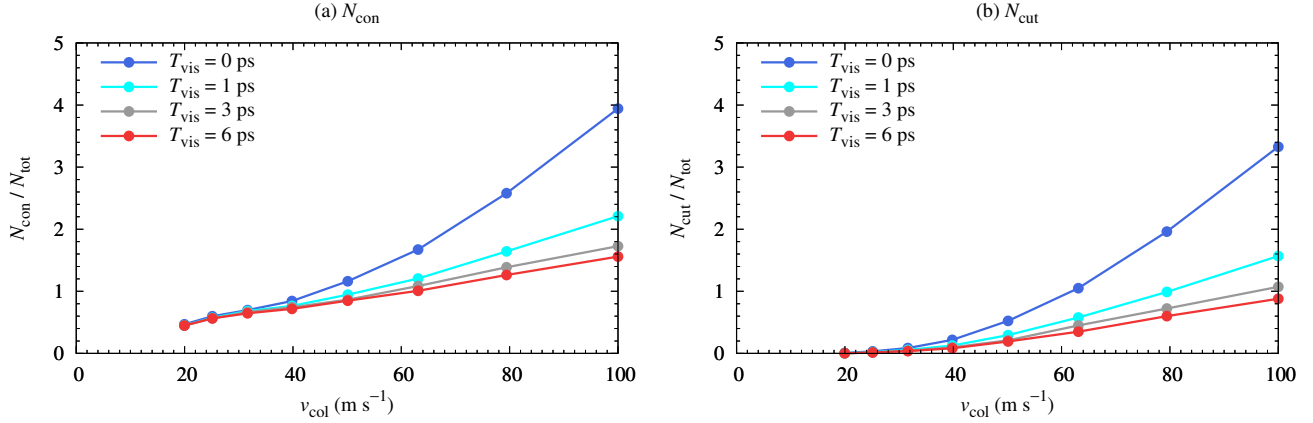


Figure 15. Numbers of connection and disconnection events in a collision between dust aggregates. (a) Number of connection events, N_{con} . (b) Number of disconnection events, N_{cut} . Here we set $B_{\text{off}}^2 = 3/12$.

however, impacts of viscous dissipation on the collisional behavior of dust aggregates have not been studied in detail.

Umstätter & Urbassek (2021b) reported that the threshold velocity increases with the strength of viscous dissipation force when we consider a head-on collision of dust aggregates. However, in reality, almost all collision events in protoplanetary disks are oblique collisions, and whether the viscous dissipation helps the collisional growth of dust aggregates is unclear.

In this study, we examined the impacts of viscous dissipation on the collisional behavior of dust aggregates. We performed numerical simulations of collisions between two equal-mass dust aggregates with various collision velocity and impact parameters. We also changed the strength of viscous dissipation force systematically, which is controlled by T_{vis} called the viscoelastic timescale (see Eq. (7)). In this study, we set that dust particles constituting dust aggregates are made of water ice, and the all particles have the same radius of $r_1 = 0.1 \mu\text{m}$. The total number of particles in a simulation is $N_{\text{tot}} = 10^5$, and both target and projectile aggregates are prepared by ballistic particle–cluster aggregation. Our key findings are summarized as follows.

1. The threshold velocity for sticking in a head-on collision of individual dust particle (v_{stick}) for $T_{\text{vis}} = 6$ ps is approximately 10 times higher than that for $T_{\text{vis}} = 0$ ps. In contrast, we found that v_{fra} barely depends on T_{vis} within the range of $0 \text{ ps} \leq T_{\text{vis}} \leq 6 \text{ ps}$ (Figure 5). This indicates that the dominant energy dissipation process for collisions of dust aggregates is different from that for head-on collisions of individual particles.
2. We analyzed the normal component of the interparticle velocity (v_{rel}) from snapshots of our numerical simulations (Figures 10–12). We found that the root mean square of v_{rel} is always lower than 1 m s^{-1} for non-zero T_{vis} , and its decrease timescale is $\simeq 0.2 \mu\text{s}$. From

a simple estimate (see Section 5.1), we confirmed that the viscous energy dissipation would not be the main mechanism for the energy dissipation for collisions between dust aggregates.

3. We also checked the total energy dissipation due to particle interactions from $t = 0$ and discussed which is the main mechanism for the energy dissipation (Figures 13 and 14). We found that the rolling friction is the main mechanism for the energy dissipation when $v_{\text{col}} \lesssim v_{\text{fra}}$, and the energy dissipation due to connection and disconnection of particles is always not the main mechanism for the energy dissipation.
4. We showed the size distribution of fragments formed after collisions (Figures 6–9). We found that largest fragments dominate the mass for all cases in this study. In addition, with non-zero T_{vis} , the largest fragments dominate not only the mass but also the surface area even for $v_{\text{col}} = 100 \text{ m s}^{-1}$. We also obtained a simple empirical fitting for the size distribution of fragments for the case of strong viscous dissipation: $f(N) \simeq N^{-1}$ (see Section 4).

As the energy dissipation due to tangential motions of particles in contact plays a key role in our simulations, we should investigate how collisional outcomes depend on the spring constants and the critical displacements for tangential motions in future studies. We also plan to perform numerical simulations of collisions between two aggregates made of non-spherical particles to demonstrate how the particle shape affects particle interactions including tangential motions.

ACKNOWLEDGMENTS

The anonymous reviewer provided a constructive review that improved this paper. The authors thank Sebastiaan Krijt

and Yukihiro Hasegawa for their helpful comments. Numerical computations were carried out on PC cluster at CfCA, NAOJ. S.A. was supported by JSPS KAKENHI Grant No.

JP20J00598. H.T. and E.K. were supported by JSPS KAKENHI Grant No. 18H05438. This work was supported by the Publications Committee of NAOJ.

REFERENCES

- Adachi, I., Hayashi, C., & Nakazawa, K. 1976, *Progress of Theoretical Physics*, 56, 1756, doi: [10.1143/PTP.56.1756](https://doi.org/10.1143/PTP.56.1756)
- Arakawa, S., & Krijt, S. 2021, *ApJ*, 910, 130, doi: [10.3847/1538-4357/abe61d](https://doi.org/10.3847/1538-4357/abe61d)
- Blum, J., & Wurm, G. 2008, *ARA&A*, 46, 21, doi: [10.1146/annurev.astro.46.060407.145152](https://doi.org/10.1146/annurev.astro.46.060407.145152)
- Brisset, J., Heielmann, D., Kothe, S., Weidling, R., & Blum, J. 2016, *A&A*, 593, A3, doi: [10.1051/0004-6361/201527288](https://doi.org/10.1051/0004-6361/201527288)
- . 2017, *A&A*, 603, A66, doi: [10.1051/0004-6361/201630345](https://doi.org/10.1051/0004-6361/201630345)
- Dominik, C., & Tielens, A. G. G. M. 1995, *Philosophical Magazine, Part A*, 72, 783, doi: [10.1080/01418619508243800](https://doi.org/10.1080/01418619508243800)
- . 1996, *Philosophical Magazine, Part A*, 73, 1279, doi: [10.1080/01418619608245132](https://doi.org/10.1080/01418619608245132)
- . 1997, *ApJ*, 480, 647, doi: [10.1086/303996](https://doi.org/10.1086/303996)
- Fritscher, M., & Teiser, J. 2021, *ApJ*, 923, 134, doi: [10.3847/1538-4357/ac2df4](https://doi.org/10.3847/1538-4357/ac2df4)
- Gundlach, B., & Blum, J. 2015, *ApJ*, 798, 34, doi: [10.1088/0004-637X/798/1/34](https://doi.org/10.1088/0004-637X/798/1/34)
- Gttler, C., Blum, J., Zsom, A., Ormel, C. W., & Dullemond, C. P. 2010, *A&A*, 513, A56, doi: [10.1051/0004-6361/200912852](https://doi.org/10.1051/0004-6361/200912852)
- Gttler, C., Heielmann, D., Blum, J., & Krijt, S. 2012, arXiv e-prints, arXiv:1204.0001. <https://arxiv.org/abs/1204.0001>
- Hasegawa, Y., Suzuki, T. K., Tanaka, H., Kobayashi, H., & Wada, K. 2021, *ApJ*, 915, 22, doi: [10.3847/1538-4357/abf6cf](https://doi.org/10.3847/1538-4357/abf6cf)
- Hayashi, C. 1981, *Progress of Theoretical Physics Supplement*, 70, 35, doi: [10.1143/PTPS.70.35](https://doi.org/10.1143/PTPS.70.35)
- Johansen, A., Blum, J., Tanaka, H., et al. 2014, in *Protostars and Planets VI*, ed. H. Beuther, R. S. Klessen, C. P. Dullemond, & T. Henning, 547, doi: [10.2458/azu.uapress.9780816531240-ch024](https://doi.org/10.2458/azu.uapress.9780816531240-ch024)
- Johnson, K. L., Kendall, K., & Roberts, A. D. 1971, *Proceedings of the Royal Society of London Series A*, 324, 301, doi: [10.1098/rspa.1971.0141](https://doi.org/10.1098/rspa.1971.0141)
- Krijt, S., Dominik, C., & Tielens, A. G. G. M. 2014, *Journal of Physics D Applied Physics*, 47, 175302, doi: [10.1088/0022-3727/47/17/175302](https://doi.org/10.1088/0022-3727/47/17/175302)
- Krijt, S., Gttler, C., Heielmann, D., Dominik, C., & Tielens, A. G. G. M. 2013, *Journal of Physics D Applied Physics*, 46, 435303, doi: [10.1088/0022-3727/46/43/435303](https://doi.org/10.1088/0022-3727/46/43/435303)
- Mizutani, H., Takagi, Y., & Kawakami, S.-I. 1990, *Icarus*, 87, 307, doi: [10.1016/0019-1035\(90\)90136-W](https://doi.org/10.1016/0019-1035(90)90136-W)
- Mukai, T., Ishimoto, H., Kozasa, T., Blum, J., & Greenberg, J. M. 1992, *A&A*, 262, 315
- Musiolik, G., Teiser, J., Jankowski, T., & Wurm, G. 2016, *ApJ*, 827, 63, doi: [10.3847/0004-637X/827/1/63](https://doi.org/10.3847/0004-637X/827/1/63)
- Nietiadi, M. L., Rosandi, Y., Branga, E. M., & Urbassek, H. M. 2022, *ApJ*, 925, 173, doi: [10.3847/1538-4357/ac403d](https://doi.org/10.3847/1538-4357/ac403d)
- Nietiadi, M. L., Rosandi, Y., & Urbassek, H. M. 2020, *Icarus*, 352, 113996, doi: [10.1016/j.icarus.2020.113996](https://doi.org/10.1016/j.icarus.2020.113996)
- Nietiadi, M. L., Umsttter, P., Tjong, T., et al. 2017, *Physical Chemistry Chemical Physics (Incorporating Faraday Transactions)*, 19, 16555, doi: [10.1039/C7CP02106B](https://doi.org/10.1039/C7CP02106B)
- Okuzumi, S., & Hirose, S. 2012, *ApJL*, 753, L8, doi: [10.1088/2041-8205/753/1/L8](https://doi.org/10.1088/2041-8205/753/1/L8)
- Ormel, C. W., & Cuzzi, J. N. 2007, *A&A*, 466, 413, doi: [10.1051/0004-6361:20066899](https://doi.org/10.1051/0004-6361:20066899)
- Paszun, D., & Dominik, C. 2009, *A&A*, 507, 1023, doi: [10.1051/0004-6361/200810682](https://doi.org/10.1051/0004-6361/200810682)
- Poppe, T., Blum, J., & Henning, T. 2000, *ApJ*, 533, 454, doi: [10.1086/308626](https://doi.org/10.1086/308626)
- Quadery, A. H., Doan, B. D., Tucker, W. C., Dove, A. R., & Schelling, P. K. 2017, *ApJ*, 844, 105, doi: [10.3847/1538-4357/aa7890](https://doi.org/10.3847/1538-4357/aa7890)
- Sakurai, Y., Ishihara, T., Furuya, H., Umemura, M., & Shiraishi, K. 2021, *ApJ*, 911, 140, doi: [10.3847/1538-4357/abe9ba](https://doi.org/10.3847/1538-4357/abe9ba)
- Schrpler, R., Blum, J., Krijt, S., & Raabe, J.-H. 2018, *ApJ*, 853, 74, doi: [10.3847/1538-4357/aaa0d2](https://doi.org/10.3847/1538-4357/aaa0d2)
- Schrpler, R. R., Landeck, W. A., & Blum, J. 2022, *MNRAS*, 509, 5641, doi: [10.1093/mnras/stab3348](https://doi.org/10.1093/mnras/stab3348)
- Seizinger, A., Krijt, S., & Kley, W. 2013, *A&A*, 560, A45, doi: [10.1051/0004-6361/201322773](https://doi.org/10.1051/0004-6361/201322773)
- Shimaki, Y., & Arakawa, M. 2012, *Icarus*, 221, 310, doi: [10.1016/j.icarus.2012.08.005](https://doi.org/10.1016/j.icarus.2012.08.005)
- Sirono, S.-i., & Kudo, D. 2021, *ApJ*, 911, 114, doi: [10.3847/1538-4357/abec7c](https://doi.org/10.3847/1538-4357/abec7c)
- Sirono, S.-i., & Ueno, H. 2017, *ApJ*, 841, 36, doi: [10.3847/1538-4357/aa6fad](https://doi.org/10.3847/1538-4357/aa6fad)
- Tanaka, H., Wada, K., Suyama, T., & Okuzumi, S. 2012, *Progress of Theoretical Physics Supplement*, 195, 101, doi: [10.1143/PTPS.195.101](https://doi.org/10.1143/PTPS.195.101)
- Umsttter, P., & Urbassek, H. M. 2020, *A&A*, 633, A24, doi: [10.1051/0004-6361/201936527](https://doi.org/10.1051/0004-6361/201936527)
- . 2021a, *A&A*, 652, A40, doi: [10.1051/0004-6361/202141581](https://doi.org/10.1051/0004-6361/202141581)
- . 2021b, *Granular Matter*, 23, 1, doi: [10.1007/s10035-021-01101-w](https://doi.org/10.1007/s10035-021-01101-w)
- Wada, K., Tanaka, H., Okuzumi, S., et al. 2013, *A&A*, 559, A62, doi: [10.1051/0004-6361/201322259](https://doi.org/10.1051/0004-6361/201322259)

Wada, K., Tanaka, H., Suyama, T., Kimura, H., & Yamamoto, T.
2007, *ApJ*, 661, 320, doi: [10.1086/514332](https://doi.org/10.1086/514332)
—, 2008, *ApJ*, 677, 1296, doi: [10.1086/529511](https://doi.org/10.1086/529511)
—, 2009, *ApJ*, 702, 1490, doi: [10.1088/0004-637X/702/2/1490](https://doi.org/10.1088/0004-637X/702/2/1490)

Weidenschilling, S. J. 1977, *MNRAS*, 180, 57,
doi: [10.1093/mnras/180.2.57](https://doi.org/10.1093/mnras/180.2.57)